



ELSEVIER

Available online at [www.sciencedirect.com](http://www.sciencedirect.com)

SCIENCE @ DIRECT®

Physics of the Earth and Planetary Interiors 149 (2005) 155–164

PHYSICS  
OF THE EARTH  
AND PLANETARY  
INTERIORS

[www.elsevier.com/locate/pepi](http://www.elsevier.com/locate/pepi)

# A case for hot slab surface temperatures in numerical viscous flow models of subduction zones with an improved fault zone parameterization

James A. Conder\*

*Department of Earth and Planetary Sciences, Washington University, Campus Box 1169, St. Louis, MO 63130, USA*

Received 28 February 2004; received in revised form 16 April 2004; accepted 26 August 2004

## Abstract

Viscous flow models play a fundamental role in our understanding of the dynamics and thermal structure of subduction zones. For example, the relatively cool slabs produced in 2D viscous flow models have been central to the argument against slab and sediment melting at subduction zones except in special cases, such as near slab edges. Because flow models have such an important role in our insight to the subduction process, it is imperative to understand how various assumptions in the models affect their results. The fault zone is a key part of subduction models, but the effects of different parameterizations on the results have been largely ignored. The two main fault parameterizations used in the literature are weak (low viscosity) nodes imposed at the fault surface and an imposed rigid overlying plate. Each formulation has pros and cons, but their only physical justification is that they keep the overlying mechanical lithosphere from deforming in unrealistic ways. Because the assigned thickness of the imposed plate or the dimensions of the weak zone governs the amount of ablation that occurs in the corner and the temperature of the material advected to the subducting slab, different arbitrary implementations can result in significantly different flow patterns and thermal structures. A fault zone parameterization with a rigid plate defined by temperature and strain rate rather than by depth or other geometry could ameliorate the predicament. This formulation removes much of the arbitrariness from the modeling, as it is based on a physical process. This formulation has the advantages of restricting viscous deformation in the overriding plate without limiting processes such as ablation by imposed boundary conditions. Model results with this parameterization show hotter slab surface temperatures than previously shown in the literature. The results also agree as well as or better than other formulations with geophysical observations such as heat flow, seismic velocity, and seismic attenuation. The calculated higher slab surface temperatures could lead to a reappraisal of sediment melting at subduction zones without requiring an atypical tectonic environment.

© 2004 Elsevier B.V. All rights reserved.

*Keywords:* Subduction; Numerical modeling; Arc magmatism; Thermal models

## 1. Introduction

Numerical and analytical viscous flow models are central in shaping our understanding of subduction

\* Tel.: +1 314 935 7372; fax: +1 314 935 7361.

*E-mail address:* [conder@seismo.wustl.edu](mailto:conder@seismo.wustl.edu).

zone dynamics and thermal structures. For instance, the thermal structure results of numerical models are often cited as primary evidence that the cold slab is not heated enough by the adjacent asthenospheric wedge to melt the subducted oceanic crust or associated sediments (e.g., Davies and Stevenson, 1992) and as evidence that frictional heating on the fault is also not likely to produce enough heat to melt the slab (e.g., Andrews and Sleep, 1974). Wedge models have helped give a better picture of the mineralogy and metamorphism in subduction zones (e.g., Peacock, 1996), and recent numerical results have demonstrated that decompression melting is a viable melting mechanism at volcanic arcs (Conder et al., 2002b). Because of its versatility, numerical modeling will undoubtedly continue as a primary tool for understanding important geological processes within the mantle wedge.

As viscous codes proliferate through the geophysical community and continue to produce insightful results regarding subduction zones, the number of studies using numerical viscous flow models is likely to increase. When designing a wedge model, every modeler must decide how to address the fault. Simply ignoring the fault by allowing complete viscous coupling between the two converging plates leads to unrealistic deformation of the overlying plate by either extreme ablation or recycling of the overlying plate, depending on the given model setup and boundary conditions. Ultimately, the best way to treat the fault zone will probably be with codes that can handle visco–elastic–plastic rheologies such as FLAC (e.g., Hall et al., 2003), especially for examining the coupling of surface dynamics with the deeper system. However, such codes are computationally expensive and do require a few a priori assumptions to implement a fault. A carefully designed viscous flow model can produce as good an examination of the wedge dynamics as more complex and unwieldy codes, but does so at the expense of dynamics in the upper plate. As many geologically important processes at subduction zones occur primarily within the wedge, this is often a small sacrifice. However, this still leaves open the question of how to properly parameterize the fault zone in such models. Two main strategies used in the literature are (1) assigning weak (reduced viscosity) nodes along the fault plane and (2) imposing a rigid upper plate by assigning a zero velocity condition to certain nodes in the overriding plate, thus restricting them from participating in the viscous

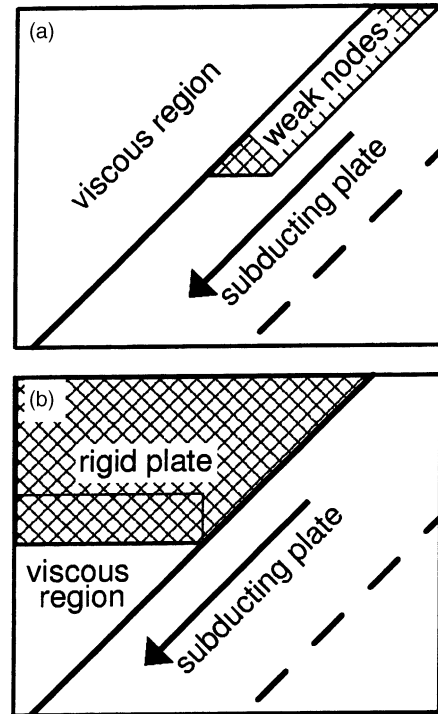


Fig. 1. Schematic representation of two commonly used wedge model parameterizations to address the fault zone. In both, nodes in the subducting plate are assigned a velocity condition to make subduction a continuous process. Parameterizations such as these shown are necessary to keep the overriding plate from complete viscous coupling across the fault. (a) The viscosity at nodes within a given region at the surface of the slabs are reduced to promote sliding along the fault and reducing the viscous deformation in the overriding plate. (b) Nodes in the upper plate are assigned a zero velocity condition, isolating them from the corner flow and allowing no deformation in the upper plate. The upper plate does not need to be of uniform thickness. For example, some studies (Peacock and Wang, 1999; van Keken et al., 2002) use an upper plate with the shape given with the outlined block removed.

flow region (Fig. 1). To implement a fault with the latter method, it is technically only necessary to fix the nodes in the upper plate directly adjacent to the fault. However, it makes intuitive sense to make a rigid plate rather than just a rigid fault, so the entire plate is typically fixed in the literature. To date, the influence of various fault parameterizations on the results has been largely ignored. This study explores the implications for the predicted thermal structures and flow patterns for the applications of the two methods listed above and the different ways of introducing the given assumptions to the models. I show that both methods give broadly

similar flow patterns, but vary significantly in details of important predictions such as slab thermal structure in the uppermost corner. I propose a modification to the rigid plate parameterization as a more realistic way to address the fault by imposing a rigid upper plate rheology with a brittle–ductile transition based on both temperature and strain rate. This method is based on more realistic physical properties of the lithosphere. This method predicts hotter slab surface temperatures than earlier models and produces results that agree as well or better with seismic and other geophysical observations at subduction zones than other parameterizations.

## 2. Wedge flow models/fault parameterizations

Analytical models of corner flow in the mantle wedge have existed almost as long as the recognition of plate tectonics (e.g., McKenzie, 1969). Analytical models implicitly assume a locked plate above an isoviscous wedge structure. Many numerical models also use an isoviscous wedge structure (e.g., Davies and Stevenson, 1992; Peacock, 1996). Isoviscous models are attractive for several reasons: they are simpler to implement, take less computing time, and are easier to compare directly to analytical and laboratory corner flow models (e.g., Becker et al., 1999). Almost invariably, the fault is addressed by imposing a rigid plate in isoviscous models. As previous workers understood, if a plate is not imposed, the isoviscous structure allows cold lithospheric material to be mobilized as easily as warmer asthenospheric material. This mobilization leads to high heat flow in the forearc (Fig. 2) and cold slab surface temperatures (SSTs) (Fig. 3) as the corner flow constantly draws cold material to the slab and thins the upper plate. The assigned thickness of the plate controls the minimum temperature of mantle material that can be easily mobilized. Thicker plates make colder forearcs and warmer SSTs at depth (Fig. 3) by trapping more relatively cool material in the rigid lithosphere. Plate thicknesses of ~40–70 km span the literature, a range that can reasonably satisfy the observed heat flow (Fig. 2).

To better capture the physical processes happening within subduction zones, temperature-dependent viscosity structures are applied in a newer generation of subduction models (Kincaid and Sacks, 1997; Eberle et al., 2002; Conder et al., 2002b; van Keken

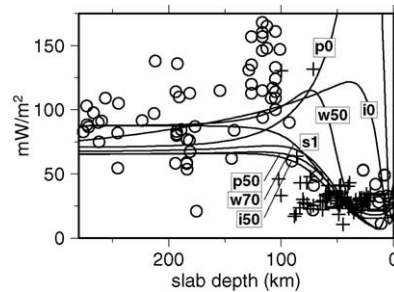


Fig. 2. Heat flow vs. slab depth. Model heat flow values (lines) are calculated at each surface grid node by assuming a conductivity of  $3 \text{ W m}^{-1} \text{ K}^{-1}$  and multiplying by  $dT/dz$ . Isoviscous models are: i0 (no plate) and i50 (50 km rigid plate). Temperature-dependent viscosity models are: p0 (no plate or weak nodes), w50 (weak nodes to 50 km depth), w70 (weak nodes to 70 km depth), p50 (rigid plate to 50 km depth), and s1 (rigid plate defined by temperature and strain rate). Symbols are data from Japan, Kermadec, and Tonga. Data from Tonga are limited to two forearc measurements from ODP (squares). Kermadec values are also largely restricted to the forearc (crosses) (Von Herzen et al., 2001). Both are similar with heat flow values from Japan (circles) (Furukawa, 1993) with low heat flow in the forearc and a rapid increase near the arc. The very high values at the arc are accentuated by advection of magma near the surface (Honda, 1985). Models allowing complete viscous coupling across the fault (i0 and p0) result in unreasonably high heat flow in the forearc which decreases towards the arc, clearly showing that some sort of parameterization of the fault zone is necessary to reduce the coupling across the fault. Beyond that, heat flow is not a strong constraint. Allowing for magma convection near the surface to explain the very high heat flow at the arc, most models with either weak nodes or rigid plates exhibit heat flow predictions of the correct magnitude for both the arc and forearc regions.

et al., 2002; Kelemen et al., 2003). (Interestingly, early models often employed temperature-dependent viscosity before isoviscous numerical models became standard practice (e.g., Andrews and Sleep, 1974; Bodri and Bodri, 1978), but unfortunately suffered somewhat from coarse resolution because of a lack of computing power.) If no plate or fault is explicitly assigned, complete viscous coupling between the subducting and overriding plates occurs. With complete viscous coupling, the high-viscosity portion of the upper plate near the slab is nearly all entrained in the downgoing system while hot, low-viscosity material is drawn to the uppermost corner of the model. Hot, upwelling material is stopped from reaching the surface only by the assigned boundary condition, resulting in excessively high heat flow in the forearc (Rowland and Davies, 1999) (Fig. 2).

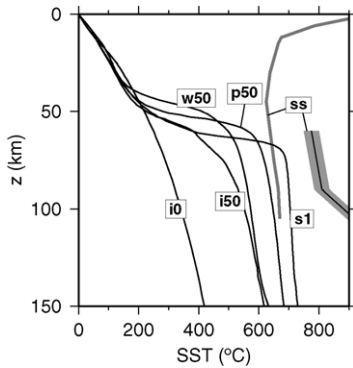


Fig. 3. Slab surface temperatures (SSTs) predicted for various models (thick lines). Model labels are same as in Fig. 2. Experimentally determined sediment solidi (ss) from Johnson and Plank (1999) (gray band) and Nichols et al. (1996) (gray line) are also plotted. Cold SSTs are often cited as an argument against any melting of the slab. As a rule, isoviscous models have cooler SSTs than temperature-dependent viscosity models. In this suite of models, the one using the most realistic fault zone parameterization (s1) exhibits the highest SSTs, suggesting that slab melting be a more common process than widely believed.

To keep this extreme ablation and penetration from occurring, both the rigid plate and weak node formulations have been applied in the various studies.

Weak nodes have been used in both larger-scale dynamic models (e.g., Gurnis and Hager, 1998) and in wedge-focused models. Larger-scale dynamic models are typically concerned more with the dynamics of the subducting and overriding plates and less with upper wedge processes than wedge-focused models and will not be discussed here. For a discussion of weak nodes on large-scale dynamic models see Chen and King (1998). Weak nodes are attractive in wedge models because the upper plate behaves entirely viscously and evolves as processes such as corner flow and ablation proceed while allowing slipping to occur at the fault, so ablation does not become a runaway process. Although the upper plate can evolve with time, the assigned dimensions of the weak zone govern the proceeding evolution. A cold corner beneath the forearc will grow to match whatever dimensions are assigned to the weak zone (i.e., an N km deep weak zone produces a cold corner to  $\sim N$  km). Similar to rigid plates, a range of  $\sim 50$ – $100$  km gives reasonable heat flow predictions (Fig. 2). Unfortunately, one attractive characteristic of weak node applications is also one of its drawbacks. Because the entire plate can behave vis-

cously, some parts of the plate deform viscously that probably should not. In particular, tractions exerted on the cold corner from below and to the side cause a slow rotation of the cold corner (although low-viscosity, the weak zone still exerts stresses on the adjacent plate). It is difficult to imagine that this process occurs in the real Earth. If so, the constant overturn should probably prevent crustal rocks from being regularly dredged in forearcs. Interestingly, this rotation actually improves the predicted fit to heat flow in forearcs, although likely for the wrong reason. The rotation homogenizes temperatures in the corner giving a flatter heat flow in the forearc (Fig. 2). The same temperature homogenization could likely occur from seawater circulation along cracks and faults throughout the forearc.

An improved parameterization, similar in philosophy to the weak node parameterization, was developed by Zhong and coworkers (Zhong and Gurnis, 1995; Zhong et al., 1998) and subsequently used by van Hunen et al. (2000, 2002). This formulation does away with the low viscosity nodes, and reduces the coupling directly with an internal boundary condition that restricts the magnitude of the shear stresses that can be transferred across the fault (normal stresses have no such restriction). This method is appealing as the underlying physics likely behaves more like a real fault than reduced viscosity nodes will. However, it too requires an a priori assignment of the fault dimensions (and magnitude of allowable shear stress transmission) which controls the thermal structure of the uppermost corner much the same way low viscosity node parameterizations do (i.e., degree of ablation limited by assigned fault length).

Because they have been widely cited, it is worth noting that the results of Kincaid and Sacks (1997) (hereafter K&S) with a temperature-dependent viscosity and weak nodes at the fault, do not show ablation of the upper plate, and therefore do not agree with more recent studies with or without weak nodes. Rather than ablation, they show a cold 'viscous nose' propagating down the surface of the slab. The disagreement arises from one of the many subtle pitfalls that modelers can encounter. Large viscosity contrasts are difficult for numerical methods to handle properly, often requiring either finer grid resolution or some simplifying assumption. For example, Bodri and Bodri (1978) assigned all nodes more viscous than a given maximum to be in the fixed mechanical

lithosphere. K&S assigned all nodes more viscous than a given maximum to that maximum value. At first glance these approaches appear to be similar, but they produce very different results. The first is a rigid plate over a temperature-dependent viscosity asthenosphere. The second is an isoviscous layer above a temperature-dependent asthenosphere. The thickness ( $z_L$ ) of the overlying isoviscous layer controls the degree of ablation. The degree of ablation can vary from extreme at  $z_L=0$  to none for larger  $z_L$ s. The cutoff value used by K&S works out to a ‘lithospheric’ thickness of just over 70 km deep ( $\sim 1150^\circ\text{C}$  isotherm). This depth inhibits ablation and has the ‘viscous nose’ effect of blanketing the slab with material that has the maximum viscosity allowed in the model.

The arbitrary nature of the implementation of the various parameterizations should not be overlooked in models with either rigid plates or weak nodes. Reasonable dimensions are weakly constrained, and implementation is largely up to modeler discretion. However, the assigned depth of the plate governs the amount of ablation occurring in the corner and the coldest temperature allowed to impinge on the plate, which in turn determines SSTs, the dimensions of the cold corner and the amount of upwelling beneath the volcanic front. Furthermore, the inferred transition between the cold corner and the hotter asthenosphere from heat flow modeling and seismic observations indicates that uppermost wedge processes are probably more complex than some parameterizations can really address. Peacock and Wang (1999) and van Keken et al. (2002) reduced the rigid plate thickness beneath the back-arc and arc relative to that adjacent to the fault (Fig. 1). This geometry is reasonably closer to that suggested by the geophysical observations and likely produces a more realistic thermal structure relative to a completely flat lithospheric base, but it is somewhat unsatisfying to match observations by locking certain nodes without a clear mechanism. It would be preferable to lock the desired nodes from a physical basis and allow the system to evolve to its preferred state. Conder et al. (2002b) reasoned that the brittle–ductile transition depends more on temperature than on depth and assigned an upper plate based on the  $800^\circ\text{C}$  isotherm. This formulation has the advantage of allowing ablation to evolve as hot incoming material heats up the base of the plate and “unlocks” nodes as they warm, but restricts penetration from becoming a runaway pro-

cess, allowing for a cold corner to develop. This is more satisfying as it has a physical basis, but is still somewhat incomplete. To reasonably satisfy the heat flow data, a temperature at the high end of that suggested for the brittle–ductile transition is necessary (typically assumed  $\sim 600\text{--}750^\circ\text{C}$  (Wiens and Stein, 1983; Kuo et al., 1986)); otherwise the hot asthenosphere penetrates too far into the corner to satisfy the heat flow. A high transition temperature may be reasonable as the brittle–ductile temperature also depends on strain rate, with the corner region of subduction zones having some of the highest strain rates anywhere. However, this single isotherm likely over-predicts the thickness of the plate in the back-arc, where strain rates are not quite as high. Also, the resulting division between the cold corner and the hot asthenosphere is not as vertically abrupt as some seismic observations suggest.

A possibly more complete way to introduce a rigid plate fault parameterization could be to consider all important factors that likely determine where the brittle–ductile transition (BDT) lies beneath the overriding plate. The BDT is defined as where the brittle strength is the same as the ductile strength. To determine the transition temperature, I assume the brittle strength,  $\tau$ , is given by the linear relationship (Byerlee, 1978),

$$\tau = 50 + 0.6\sigma_N \quad (1)$$

where  $\sigma_N$  is the normal stress and  $\tau$  and  $\sigma_N$  are in units of MPa. Assuming deformation from dislocation creep (Karato and Wu, 1993), the ductile strength,  $\sigma$ , is given by

$$\sigma = \left\{ \mu^n \dot{\epsilon} A^{-1} \exp \left[ \frac{E^* + P v^*}{RT} \right] \right\}^{1/n} \quad (2)$$

where  $\mu$  is the shear modulus,  $\dot{\epsilon}$  the strain rate,  $E^*$  the activation energy,  $v^*$  the activation volume,  $R$  the gas constant,  $T$  the temperature in Kelvins,  $n$  the stress exponent, and  $A$  a pre-exponential constant. Using the values for  $\mu$ ,  $A$ ,  $n$ ,  $E^*$ , and  $v^*$  from Karato and Wu (1993) and assuming a strain rate and a plate age, the temperature and pressure of the BDT can be determined using the above relationships. Although the transition is likely more complex than the intersection of Eqs. (1) and (2) implies, this simple transition suffices for a first-order approximation. By varying the plate age (geotherm) and assumed strain rate, some trends become apparent. Depending on the strain rate, the BDT

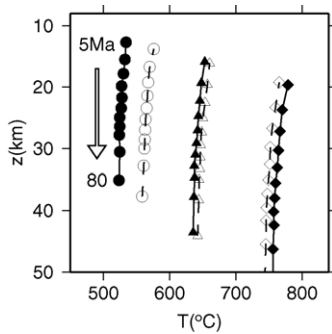


Fig. 4. Depth and temperature of brittle–ductile transition for various plate ages (geotherms), and strain rates from the equations in the text. Identical symbols indicate a constant strain rate (circles:  $10^{-17} \text{ s}^{-1}$ ; triangles:  $10^{-14} \text{ s}^{-1}$ ; diamonds:  $10^{-11} \text{ s}^{-1}$ ) but differing plate ages varying from a 5 to 80 Myr old plate. Filled symbols denote ‘wet’ rheology and open symbols denote ‘dry’ rheology of Karato and Wu (1993). Even with large changes in plate thickness, the transition temperature does not change much for a given strain rate, showing that pressure has a minor effect on the transition, while temperature can vary nearly  $200^\circ\text{C}$  with changing strain rate.

temperature can vary  $200^\circ\text{C}$  or more, while pressure has a negligible effect (Figs. 4 and 5). A good rule of thumb is that the BDT temperature increases  $\sim 33^\circ\text{C}$  per order of magnitude increase in strain rate (Fig. 5). By using this simple relationship, a rigid plate can be prescribed while still allowing the system to evolve to its own preferred state. Admittedly, convergence to steady-state often takes longer with this formulation,

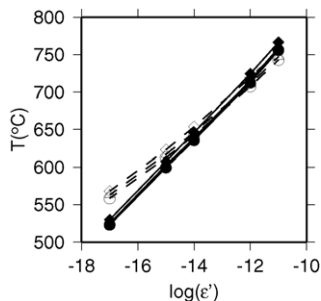


Fig. 5. Brittle–ductile transition temperature vs.  $\log$  strain rate for fixed plate ages. Diamonds: 20 Myr old plate; triangles: 40 Myr old plate, and circles: 80 Myr old plate. Filled symbols denote ‘wet’ rheology and open symbols denote ‘dry’ rheology. The transition temperature varies nearly linearly with  $\log$  strain rate. This simple relationship is convenient for implementation of a temperature–strain rate-dependent rigid plate in viscous wedge flow models.

but that is expected as the flow field is less constrained by initial conditions. In practice it may be useful to define a maximum transition temperature. As node spacing becomes small, the calculated strain rate between nodes across the fault, and therefore the transition temperature, could become unreasonably large. The maximum transition temperature for the model presented here is  $<800^\circ\text{C}$ , therefore, it was not necessary to assign a maximum transition temperature.

### 3. Methods

To investigate how the thermal structure in the mantle wedge varies with different fault parameterizations, I develop a simple 2D kinematic viscous flow model and systematically vary only the treatment of the fault zone, then compare the results of the different conditions after steady-state is reached. I use  $500 \text{ km}$  wide  $\times$   $400 \text{ km}$  deep model space with  $121 \times 81$  nodes with variable spacing to give best resolution near the corner. Node spacing near the corner is  $\sim 1 \text{ km}$  while that nearer the edges is closer to  $10\text{--}15 \text{ km}$ . The FORTRAN code has been used in several previous studies of Parmentier and coworkers (Jha et al., 1994; Braun et al., 2000; Conder et al., 2002a). The flow field is solved with a finite-element penalty function method, while the temperature field is solved with finite-differences. Boundary conditions are constant throughout the models in this paper. So resulting differences can be attributed to the fault zone parameterization. Velocities along the surface of the upper plate are set to zero, while those in the slab colder than  $750^\circ\text{C}$  are assigned to subduct at an intermediate rate of  $6 \text{ cm/year}$  at a dip angle of  $45^\circ$ . The sides and bottom are stress free. Initial plate thermal structures are calculated using the error function assuming a given plate age and a background mantle potential temperature of  $1350^\circ\text{C}$ . The incoming plate is given a thermal structure of a 50 Myr old plate, which is assigned as the plate enters the model through the right edge. At the time of subduction initiation, the overriding plate has the thermal structure of a 10 Myr old plate, but can grow with time. When applied, weak nodes (viscosity reduction of three orders of magnitude) have a width of  $20 \text{ km}$  and extend to a specified depth along the top of the subducting plate. I neglect buoyancy forces to make the model comparisons more straightforward.

#### 4. Discussion

Heat flow predictions for five temperature-dependent viscosity models with different fault zone parameterizations and two isoviscous models with 0 and 50 km thick rigid plates are shown in Fig. 2 along with heat flow data from Japan (Furukawa, 1993) and Kermadec (Von Herzen et al., 2001). The most robust characteristic of heat flow at subduction zones is low heat flow (20–40 mW/m<sup>2</sup>) in the forearc with a rapid jump near the volcanic arc (>80 mW/m<sup>2</sup>) (Blackwell et al., 1982; Honda, 1985; Furukawa, 1993; Von Herzen et al., 2001). Heat flow is not a very tight constraint on thermal models. Many different formulations can reasonably fit the data (Fig. 2), especially considering that many of the highest heat flow values near the volcanic arc result from magma advection near the surface (Honda, 1985), which is not addressed in such models. The most robust constraint from heat flow is that the cold corner reaches to at least 40–50 km depth, but not greater than 90–100 km. Models with thinner overriding plates or shallower weak nodes predict too high heat flow in the forearc, while models with thicker plates or deeper weak nodes predict unreasonably low heat flow beneath the arc and make it very difficult to generate melt beneath the volcanic arc.

Both heat flow and the lack of high-temperature volcanism in forearcs suggest a cold upper corner beneath the forearc, but perhaps the best constraints on the dimensions of the cold corner come from seismic studies. Seismic attenuation (Roth et al., 1999; Tsumura et al., 2000; Takunami et al., 2000), velocity (Research Group, 1977), and the distribution of earthquakes above the slab (Hasegawa et al., 1994; Miura et al., 2003) all suggest a fairly sharp, vertical transition between hot asthenospheric mantle beneath the arc and cold lithospheric mantle beneath the forearc. Not only do tomographic studies show a vertical division in seismic properties beneath the arc and forearc (Roth et al., 1999; Tsumura et al., 2000; Takunami et al., 2000), the differences are noticeable in the raw data. Fig. 6 shows waveforms at two nearby stations in Tonga for the same slab earthquake. Raypaths are close to vertical beneath both stations. Although the event source is closer to Tofua in the volcanic arc, the arc arrivals are clearly more attenuated than the arrivals at Ha'apai in the forearc. This difference in waveforms highlights the contrasting seismic proper-

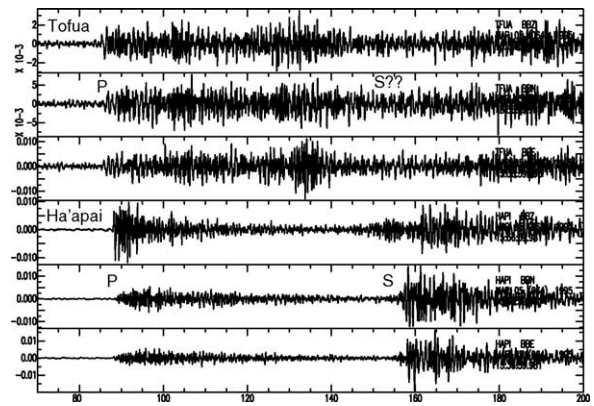


Fig. 6. Waveforms for a 600 km deep earthquake at nearby arc (Tofua) and forearc (Ha'apai) stations in Tonga (~70 km spacing). The three traces for each show, from top to bottom, the vertical, north, and east components of ground motion. Waveforms are highpass filtered at 0.6 Hz to reduce ambient 'island noise'. Both P and S wave arrivals at Tofua are noticeably more attenuated than those at Ha'apai. The raypaths for the arrivals at the two stations sample much of the same earth structure along the deeper portions of their raypaths before diverging in the wedge, so there must be a strongly attenuative region beneath Tofua that does not extend beneath Ha'apai.

ties of the arc and forearc, and suggests a clear division between them. Conductive cooling from both the upper plate and the cold slab keeps the uppermost corner fairly cold as long as asthenosphere is not allowed to penetrate far in to the corner. However, conductive cooling alone produces a gentler, non-vertical gradient between the cold corner and hotter material beneath the arc than inferred from the seismic studies. That seismic studies show a sharper transition than conductive cooling predicts suggests that asthenospheric flow approaching the corner helps control the observed shape of the transition, which, in turn, is influenced by the viscous coupling/uncoupling transition at the fault zone.

A comparison of  $Q$  predictions (1/attenuation) shows that the various parameterizations develop vertical transitions of varying quality between the cold corner and asthenosphere beneath the arc. As  $Q$  is dependent on temperature and pressure, it is possible to convert the resultant 2D temperature fields of each model into  $Q$  predictions. Although  $Q$  beneath the forearc is much larger than  $Q$  beneath the arc (e.g., Fig. 6),  $Q$  beneath the forearc is probably reduced relative to the slab from the presence of fluids and/or serpentization. The complexities associated with seismic observations, such as  $Q$ , make the model

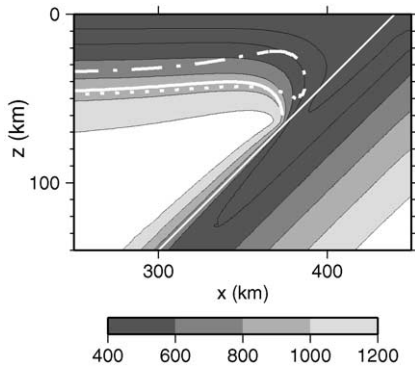


Fig. 7. Temperature and flow field for model with temperature–strain rate dependent rigid plate. Grayscale denotes temperature, with thin black lines as isotherms. Thin white line denotes the top of the slab. Thick white lines show the predicted transition from high to low attenuation for four different models. The transition defined here is where  $Q = 500$ . The exact magnitude is not crucial, as there is a rapid change in  $Q$  from the asthenosphere ( $<200$ ) to the cold corner ( $<1000$ ). The temperature–strain rate formulation (solid) and weak nodes extended to 50 km depth (dot-dashed) both exhibit reasonably sharp, vertical divisions between the low attenuation cold corner and the high attenuation asthenosphere beneath the arc, consistent with seismic observations. Models with a rigid plate defined at 50 km depth (dotted) has a sharply defined cold corner, but the transition is less vertical.

results suggestive rather than diagnostic, but a qualitative comparison can serve as a useful guide. Excluding the effects of fluids and serpentinization,  $Q$  can be approximated by the relationship (Sato et al., 1992)

$$Q = Q_{\text{pm}} \exp \left[ k \left( \frac{T_{\text{m}}}{T} - a \right) \right] \quad (3)$$

where  $Q_{\text{pm}}$  is  $Q$  at the melting temperature,  $k$  and  $a$  are constants, and  $T_{\text{m}}$  is the melting temperature in Kelvins.  $Q_{\text{pm}}$ ,  $k$ , and  $a$  values used in the calculations are those given by Sato et al. (1992). Pressure dependence comes through  $Q_{\text{pm}}$ , which is linearly dependent on pressure. For the melting temperature, I assume a linear solidus of  $1100 + 3.5 \text{ }^{\circ}\text{C}/\text{km}$ . The transition from low to high  $Q$  in the corner is rapid, so the exact shape of the solidus is not crucial. Because important controls on the magnitude of  $Q$  in the forearc are neglected, the shape of the transition is more robust than the absolute values. The calculations show that weak nodes can produce a sharp, fairly vertical transition when applied to 60 km or less, but depth-dependent rigid plates do not result in a vertical transition (Fig. 7) unless the geometry is imposed a priori on the lithosphere (e.g.,

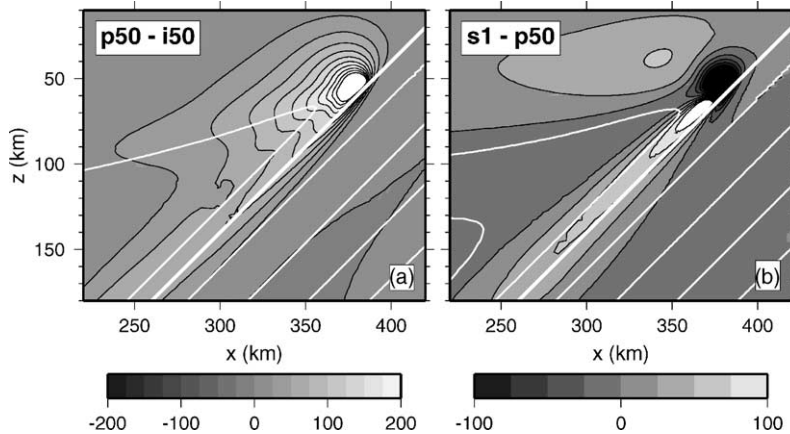


Fig. 8. Temperature difference fields showing direct comparisons between models. Gray scale is in  $^{\circ}\text{C}$ . Streamlines are shown for temperature-dependent viscosity model (p50) and strain rate-dependent fault model (s1), respectively. (a) Model with constant viscosity and a 50 km thick plate (i50) subtracted from a model with temperature-dependent viscosity and a 50 km thick plate. Slab surface temperatures are increased 100–300  $^{\circ}\text{C}$ , depending on location along the slab surface. The largest temperature differences occur in the uppermost corner where cold ‘lithospheric’ material is advected to the slab in the constant viscosity case and hot asthenospheric material is advected in the temperature-dependent viscosity case. (b) Model with temperature-dependent viscosity and 50 km thick plate subtracted from model with strain rate-dependent fault. While the temperature dependent viscosity model with a rigid plate increases the predicted slab surface temperatures, applying a more realistic fault zone parameterization increases the temperatures even more (100–150  $^{\circ}\text{C}$ ), suggesting that slab surface temperatures have been largely underestimated in most numerical, 2D, viscous flow models.

van Keken et al., 2002). A temperature and strain rate parameterization combines the best qualities of the other parameterizations by locking nodes near the fault and allowing thermal and viscous ablation of the overlying plate just behind the locked nodes. This results in a reasonably well-developed cold corner with a reasonably sharp vertical transition between asthenosphere and lithosphere in the upper corner as seen in seismic attenuation and velocity predictions (Fig. 7).

A crucial implication of this improved fault parameterization is a marked increase in predicted slab surface temperatures. Simply changing from an isoviscous rheology to a temperature-dependent rheology results in 100–300 °C warmer predicted slab surface temperatures (Fig. 8a). The temperature and strain rate dependent parameterization results in SSTs 100–150 °C warmer still (Fig. 8b). In fact, the more realistic fault zone model results in warmer SSTs than any of the previously used parameterizations, leading to the possibility that some degree of slab melting (Fig. 3) could be feasible in some arcs without resorting to special cases such as near slab edges or subduction of extremely young lithosphere. Any shear heating associated with the fault (e.g., Peacock et al., 2004) could further increase SSTs and the likelihood of slab melting. Johnson and Plank (1999) argue that sediment melting must be a ubiquitous process at subduction zones to satisfy the trace element signatures (particularly Th and Be) in arc basalts. These trace element signatures may soon be reconciled with the thermal models as increasingly realistic wedge flow models seem to predict ever-increasing slab surface temperatures.

## 5. Summary

As many of the most geologically important processes in subduction zones occur in the mantle wedge, models of wedge flow need to be carefully constructed or we as a community may learn incorrect or incomplete lessons about wedge processes. Although parameterization of the fault zone and the transition from uncoupled to coupled viscous flow significantly influences the dynamics and other results obtained from numerical viscous flow models, its importance has not been fully appreciated. Formulations such as weak nodes at the fault interface or geometrically defined rigid plates give broadly similar results, but

can still differ considerably in important details (e.g., compare w50 and p50 in Fig. 2).

Because key details can change significantly with different parameterizations, it is important to reduce the arbitrariness imposed in the models and determine which formulation most closely mimics the Earth. A rigid plate defined on the dual basis of strain rate and temperature moves toward this standard, as it has a physically viable justification and allows the model to evolve to a steady-state solution without bumping into arbitrarily forced conditions that artificially limit its behavior. A temperature and strain rate dependent fault zone gives a pronounced cold corner with the shape and dimensions consistent with that inferred from seismic velocity, seismic attenuation, and heat flow studies. Predicted slab surface temperatures are higher for this formulation than for other widely used formulations. With progressively smaller differences in the literature between predicted slab surface temperatures and the experimentally determined sediment solidus, it may be worth revisiting questions regarding slab melting in the context of thermal modeling.

## Acknowledgements

Thanks to Peter van Keken for hosting the MAR-GINS numerical modeling workshop, creating a thought-provoking forum for discussing modeling issues, and to Doug Wiens for insightful discussions. Thanks to Scott King, Peter van Keken, and Kelin Wang whose thoughtful reviews greatly improved this paper. I also thank my wife, Tami, for proofreading and for making worthwhile suggestions. This study was supported by NSF grants OCE-0002527 and OCE-0305292.

## References

- Andrews, D.J., Sleep, N., 1974. Numerical modelling of tectonic flow behind island arcs. *Geophys. J. R. Astr. Soc.* 38, 237–251.
- Becker, T.W., Faccenna, C., O'Connell, J., 1999. The development of slabs in the upper mantle: insights from numerical and laboratory experiments. *J. Geophys. Res.* 104, 15207–15226.
- Blackwell, D.D., Bowen, R.G., Hull, D.A., Riccio, J., Steele, J.L., 1982. Heat flow, arc volcanism, and subduction in northern Oregon. *J. Geophys. Res.* 87, 8735–8754.
- Bodri, L., Bodri, B., 1978. Numerical investigation of tectonic flow in island-arc areas. *Tectonophysics* 50, 163–175.

- Braun, M.G., Hirth, G., Parmentier, E.M., 2000. The effects of deep damp melting on mantle flow and melt generation beneath mid-ocean ridges. *Earth Plan. Sci. Lett.* 176, 339–356.
- Byerlee, J., 1978. Friction of rocks. *Pageoph* 116, 615–626.
- Chen, J., King, S.D., 1998. The influence of temperature and depth dependent viscosity on geoid and topography profiles from models of mantle convection. *Phys. Earth Planet Int.* 106, 75–92.
- Conder, J.A., Forsyth, D.W., Parmentier, E.M., 2002a. Asthenospheric flow and the asymmetry of the East Pacific Rise, MELT area. *J. Geophys. Res.* 107, 2344, doi:10.1029/2001JB000807.
- Conder, J.A., Wiens, D.A., Morris, J., 2002b. On the decompression melting structure at volcanic arcs and back-arc spreading centers. *Geophys. Res. Lett.*, 29, doi:10.1029/2002GL015390.
- Davies, J.H., Stevenson, D.J., 1992. Physical model of source region of subduction zone volcanics. *J. Geophys. Res.* 97, 2037–2070.
- Eberle, M.A., Grasset, O., Sotin, C., 2002. A numerical study of the interaction between the mantle wedge, subducting slab and over-riding plate. *Phys. Earth Planet Int.* 134, 191–202.
- Furukawa, Y., 1993. Depth of the decoupling interface and thermal structure under arcs. *J. Geophys. Res.* 98, 20005–20013.
- Gurnis, M., Hager, B., 1998. Controls on the structure of subducted slabs. *Nature* 335, 317–321.
- Hall, C.E., Gurnis, M., Sdrolias, M., Lavie, L.L., Muller, R.D., 2003. Catastrophic initiation of subduction following forced convergence at transform boundaries. *Earth Planet Sci. Lett.* 212, 15–30.
- Hasegawa, A., Horiuchi, S., Umino, N., 1994. Seismic structure of the northeastern Japan convergent margin: a synthesis. *J. Geophys. Res.* 99, 22,295–22,311.
- Honda, S., 1985. Thermal structure beneath Tohoku, northeast Japan - a case study for understanding the detailed thermal structure of the subduction zone. *Tectonophysics* 112, 69–102.
- Jha, K., Parmentier, E.M., Phipps Morgan, J., 1994. The role of mantle-depletion and melt-retention buoyancy in spreading-center segmentation. *Earth Planet Sci. Lett.* 125, 221–234.
- Johnson, M.C., Plank, T., 1999. Dehydration and melting experiments constrain the fate of subducted sediments, *Geochem. Geophys. Geosyst.*, 1, 1999GC000014.
- Karato, S.-I., Wu, P., 1993. Rheology of the upper mantle: a synthesis. *Science* 260, 771–778.
- Kelemen, P.B., Rilling, J.L., Parmentier, E.M., Mehl, L., Hacker, B.R., 2003. Thermal structure due to solid-state flow in the mantle wedge beneath arcs. *Am. Geophys. U. Monogr.*, 138.
- Kincaid, C., Sacks, I.S., 1997. Thermal and dynamical evolution of the upper mantle in subduction zones. *J. Geophys. Res.* 102, 12295–12315.
- Kuo, B.-Y., Forsyth, D.W., Parmentier, E.M., 1986. Flexure and thickening of the oceanic lithosphere at the East Pacific Rise. *Geophys. Res. Lett.* 13, 681–684.
- McKenzie, D.P., 1969. Speculations on the consequences and causes of plate motions. *Geophys. J. R. Astr. Soc.* 18, 1–32.
- Miura, S., Kodaira, S., Nakanishi, A., Tsuru, T., Takahashi, N., Hirata, N., Kaneda, Y., 2003. Structural characteristics controlling the seismicity crustal structure of southern Japan trench fore-arc region, revealed by ocean bottom seismograph data. *Tectonophysics* 363, 79–102.
- Nichols, G.T., Wyllie, P.J., Stern, C.R., 1996. Experimental melting of pelagic sediment constraints relevant to subduction. In: Bebout, G.E., Scholl, D.W., Kirby, S.H., Platt, J.P. (Eds.), *Subduction Top to Bottom*, 96. AGU Monogr, pp. 293–298.
- Peacock, S.M., 1996. Thermal and petrologic structure of subduction zones. In: Bebout, G.E., Scholl, D.W., Kirby, S.H., Platt, J.P. (Eds.), *Subduction Top to Bottom*, 96. AGU Monogr, pp. 119–133.
- Peacock, S.M., Wang, K., 1999. Seismic consequences of warm versus cool subduction metamorphism: examples from southwest and northeast Japan. *Science* 286, 937–939.
- Peacock, S.M., van Keken, P., Holloway, S.D., Hacker, B.R., Abers, G.A., Ferguson, R.L., 2004. Thermal structure of the Costa Rica – Nicaragua subduction zone, *Phys. Earth and Planet. Int.*, this issue.
- Research Group for Explosion Seismology, 1977. Regionality of the upper mantle around northeastern Japan as derived from explosion seismic observations and its seismological implications, *Tectonophysics*, 37, 117–130.
- Roth, E.G., Wiens, D.A., Dorman, L.M., Hildebrand, J., Webb, S.C., 1999. Seismic attenuation tomography of the Tonga-Fiji region using phase pair methods. *J. Geophys. Res.* 104, 4795–4809.
- Rowland, A., Davies, J.H., 1999. Buoyancy rather than rheology controls the thickness of the overriding mechanical lithosphere at subduction zones. *Geophys. Res. Lett.* 26, 3037–3040.
- Sato, H., Sacks, I.S., Murase, T., Muncill, G., Fukuyama, H., 1992.  $Q_p$ -melting temperature relation in peridotite at high pressure and temperature: attenuation mechanism and implications for the mechanical properties of the upper mantle. *J. Geophys. Res.* 94, 10647–10661.
- Takanami, T., Sacks, I.S., Hasegawa, A., 2000. Attenuation structure beneath the volcanic front in northeastern Japan from broad-band seismograms. *Phys. Earth Planet Int.* 121, 339–357.
- Tsumura, N., Matsumoto, S., Horiuchi, S., Hasegawa, A., 2000. Three-dimensional attenuation structure beneath the northeastern Japan arc estimated from spectra of small earthquakes. *Tectonophysics* 319, 241–260.
- Wiens, D.A., Stein, S., 1983. Age dependence of intra-oceanic seismicity and implications for lithospheric evolution. *J. Geophys. Res.* 88, 6455–6468.
- van Hunen, J., van den Berg, A.P., Vlaar, N.J., 2000. A thermo-mechanical model of horizontal subduction below an overriding plate. *Earth Planet Sci. Lett.* 182, 157–169.
- van Hunen, J., van den Berg, A.P., Vlaar, N.J., 2002. On the role of subducting oceanic plateaus in the development of shallow flat subduction. *Tectonophysics* 352, 317–333.
- van Keken, P.E., Kiefer, B., Peacock, S.M., 2002. High-resolution models of subduction zones: implications for mineral dehydration reactions and the transport of water into the deep mantle. *Geochem. Geophys. Geosyst.*, 3, doi:10.1029/2001GC000256.
- Von Herzen, R., Ruppel, C., Molnar, P., Nettles, M., Nagihara, S., Ekström, G., 2001. A constraint on the shear stress at the Pacific-Australian plate boundary from heat flow and seismicity at the Kermadec forearc. *J. Geophys. Res.* 106, 6817–6833.
- Zhong, S., Gurnis, M., 1995. Mantle convection with plates and mobile, faulted plate margins. *Science* 267, 838–843.
- Zhong, S., Gurnis, M., Moresi, L., 1998. Role of faults, nonlinear rheology, and viscosity structure in generating plates from instantaneous mantle flow models. *J. Geophys. Res.* 103, 15255–15268.